Aerospace Science and Technology 94 (2019) 105383

Contents lists available at ScienceDirect

Aerospace Science and Technology

www.elsevier.com/locate/aescte

Effect of film cooling injection on aerodynamic performances of scramjet isolator

Kuan Zheng [a], Wei Tian [a,*], Jiang Qin [b,*], Silong Zhang [b], Hui Hu [c]

[a] School of Aeronautics and Astronautics, Shanghai Jiao Tong University, Shanghai, 200240, China
[b] School of Energy Science and Engineering, Harbin Institute of Technology, Heilongjiang 150001, China
[c] Department of Aerospace Engineering, Iowa State University, Ames, IA, 50010, United States

ARTICLE INFO

Article history:
Received 12 January 2019
Received in revised form 2 September 2019
Accepted 3 September 2019
Available online 6 September 2019

Keywords:
Film cooling injection
Scramjet engine
Isolator
Aerodynamic performances
Cooling effectiveness

ABSTRACT

With continuous increase in flight Mach number, aerodynamic heating on scramjet isolators becomes increasingly pronounced. Consequently, a thermal protection technique for scramjet isolators is urgently required. In the present study, a numerical investigation was conducted to evaluate the feasibility of applying film cooling on a scramjet isolator. First, the heat transfer characteristics under different coolant flow conditions (i.e., coolant Mach number, coolant total temperature, and injection position) were obtained to evaluate the film cooling efficiency on a scramjet isolator. Next, the characteristics of maximum backpressure and friction drag were analyzed to obtain the effects of film cooling injection on the aerodynamic performances of the scramjet isolator. It was found that the film cooling injection under proper coolant flow conditions could reduce the friction drag and enhance the ability of the isolator to resist backpressure, which is beneficial to the performances of a scramjet engine. In general, the results obtained in this study indicated that film cooling injection could be a practical thermal protection technique for a scramjet isolator.

1. Introduction

As a key component of airbreathing hypersonic vehicles, a scramjet engine typically operates under an extremely high temperature [1]. Consequently, thermal protection techniques have to be applied to avoid the thermal damage of scramjet engine materials. Many studies have been performed to develop various cooling techniques for scramjet engines, such as regenerative cooling [2–4], film cooling [5–9], and combined cooling [10,11]. Most previous studies focused on the cooling of the combustion chamber, which experiences the highest temperature in a scramjet engine. For example, Taddeo et al. [4] systematically studied the dimensioning of automated regenerative cooling in a combustion chamber. However, with the continuously increasing flight Mach number, aerodynamic heating would cause a significant heat load in the interior of a scramjet isolator. As reported by Rodriguez [11], the peak surface temperature on the isolator under a flight Mach number of 6.4 could reach 1600 K. Such a high temperature is well beyond the endurable temperature of the isolator material. Thus, the thermal protection for a scramjet isolator cannot be ignored.

During hypersonic flight, the pressure increase induced by an intense turbulent combustion leads to the formation of a shock wave train. The primary function of a scramjet isolator is to prevent the scramjet inlet from the shock wave train caused by the combustion pressure increase. Carroll and Dutton [12,13] obtained a picture of shock wave train in a rectangular duct using an improved oil-flow visualization technique. The effects of surface boundary layer and backpressure on the shock wave train were analyzed symmetrically. To improve the performance of the isolator, several methods were proposed to control the shock wave train in the isolator. For example, Tam et al. [14] and Lin et al. [15] introduced a swept ramp in an isolator and indicated that the unique pressure distribution generated by the swept ramp could enhance the isolator performance. Kouchi et al. [16], Chang et al. [17], and Chang and Fan [18] proposed a distributed flow control system that involves mass removal from the walls of the entire isolator. Their simulation results demonstrated that the unstart shock can be forced to translate downstream by removing the mass from the walls of the isolator. He et al. [19] applied surface suction control in a constant-area rectangular isolator with asymmetry nozzle. They found that the length of the shock train in the isolator can be effectively shortened by the suction.

In particular, a number of studies indicated that the wall temperature could influence the shock wave train in an isolator. Cuffel

* Corresponding authors.
E-mail addresses: tianwei@sjtu.edu.cn (W. Tian), qinjiang@hit.edu.cn (J. Qin).

https://doi.org/10.1016/j.ast.2019.105383
1270-9638/

Nomenclature

Ma	Mach number		
T	temperature	K	
T_r	recovery temperature	K	
T_{aw}	adiabatic wall temperature	K	
M	blowing ratio		
P	static pressure	Pa	
$P_{b,max}$	maximum backpressure	Pa	
η	film cooling effectiveness		
TI	turbulence intensity of the main flow		
m	mass flow rate	kg/s	
τ	axial shear stress	Pa	
F_f	friction drag	N	
x	axial coordinate		
x_c	axial coordinate of the injection position		
s	width of the injection slot		
l	length of the injection slot		
ρ	air density	kg/m^3	
μ	air viscosity coefficient		
C_p	air heat capacity		
λ	air thermal conductivity		

Subscripts

∞	freestream condition
c	coolant flow condition
$main$	condition of main flow in the isolator

and Back [20] observed the increase in shock train length with wall temperature. Lin et al. [21] found that heat addition to an isolator can choke the flow and potentially deteriorate the isolator performance. Fischer et al. [22] and Fischer and Oliver [23] experimentally studied the variation in pressure distribution in the shock train by heating the isolator surface and indicated that the boundary layer separation became more evident at a higher wall temperature. Meanwhile, several researchers found that decreasing the surface temperature using surface cooling is beneficial to the isolator performance. Spaid and Frishett [24], Back and Cuffel [25], and EI-Hady and Verma [26] reported that surface cooling can delay the boundary layer separation and reduce the interaction between the shock wave and boundary layer. Chang et al. [27] indicated that the mass-captured coefficient, total-pressure recovery coefficient, and flow uniformity at the isolator exit were improved by surface cooling. In general, surface cooling can be used to avoid the thermal damage of isolator materials, in addition to improving scramjet isolator performances.

As we mentioned, the flow structures in an isolator are complicated owing to the shock wave train and the interaction between the shock wave and boundary layer. The surface cooling technique should be introduced to ensure that the cooling technique will not deteriorate the flow environments and isolator performances. While many cooling techniques have been proposed, film cooling injection might be an appropriate choice for isolator surface cooling owing to its simple structure design that ensures a good structural integrity of the isolator surface [28–30]. In addition, the principle of film cooling injection is to generate a thin coolant blanket over the isolator surface, which is similar to boundary layer blowing. Viswanath et al. [31] conducted a wind tunnel test to evaluate supersonic boundary layer control using surface blowing. They found that surface blowing can delay the separation of the boundary layer induced by shock waves. He et al. [32] indicated that the boundary layer ejecting can increase the resistance to backpressure in an inlet isolator. Moreover, Cary and Hefner [33] experimentally investigated film cooling on a cylindrical scramjet combustor and found that film cooling could reduce viscous drag at low values of the total equivalence ratio.

While film cooling is primarily applied on a combustion chamber, studies related to using film cooling on a scramjet isolator are quite limited. Only Zhang et al. [34] numerically analyzed the film cooling effectiveness in a hypersonic inlet with an isolator. However, compared to cooling effectiveness, the effect of film cooling injection on the aerodynamic performances of a scramjet isolator should be more important. Hence, a numerical investigation was conducted in the present study with the primary purpose of evaluating the feasibility of applying film cooling on a scramjet isolator. The heat transfer characteristics under different coolant flow conditions (i.e., coolant Mach number, coolant total temperature, and injection position) were obtained to reveal the film cooling effectiveness. More importantly, the characteristics of maximum backpressure and friction drag are analyzed herein to evaluate the effects of film cooling injection on the aerodynamic performances of a scramjet isolator.

2. Physical model and computations

2.1. Physical model

Based on the axisymmetric scramjet engine used in the Central Institute of Aviation Motors/NASA flight tests [11], the same isolator combined with a hypersonic inlet was adopted as the physical model in the present study to reflect the real flow fields in the scramjet isolator. The geometric parameters of the studied model and the computational domain are shown in Fig. 1. As shown in the figure, the inlet is of mixed compression, including three external shocks and two internal shocks. The entrance height of the scramjet isolator is 11 mm. The length of the isolator is seven times the height of the isolator.

As shown in Fig. 2, the coolant flow of film cooling is injected into the isolator through a slot on the lower wall of the isolator. The width and length of the slot were set as $s = 2$ mm and $l = 18.67$ mm, respectively. The effects of film cooling injection angle on the main flow environments have been reported by several researchers [34–37]. They indicated that the injection coolant flow would induce shock waves and flow separation in the main flow, which will deteriorate the main flow environments. And this phenomenon will become more and more evident with the increase of injection angle [34,36]. Therefore, the injection angle should be small enough to minimize the effect of injection flow on the main flow environments. As shown in Figs. 1 and 2, under the restriction of the compression angle at the isolator entrance (i.e., 12.6°), the injection angle was designed to be 15° in the present study. In addition, four positions downstream the entrance of the isolator with $x_c = 475$ mm, 481 mm, 487 mm, and 493 mm were selected to investigate the effect of injection position on the film cooling effectiveness and aerodynamic performances of the scramjet isolator.

2.2. Numerical method

The computations were performed using a finite-volume integration scheme to solve the axisymmetric form of the compressible Reynolds-Averaged Navier-Stokes (RANS) equations with a double precision solver. The second-order spatially upwind scheme with the Advection Upstream Splitting Method (AUSM) flux vector was

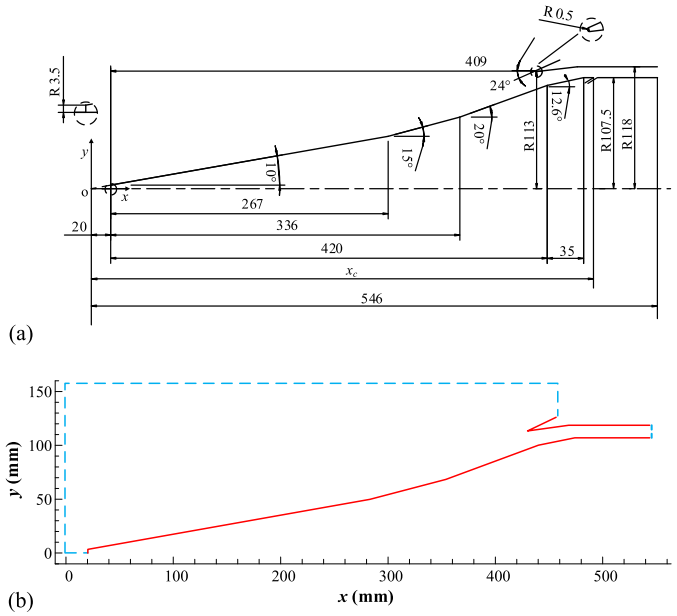

Fig. 1. Isolator model (a) schematic of the scramjet isolator with hypersonic inlet (units: mm); (b) computational domain.

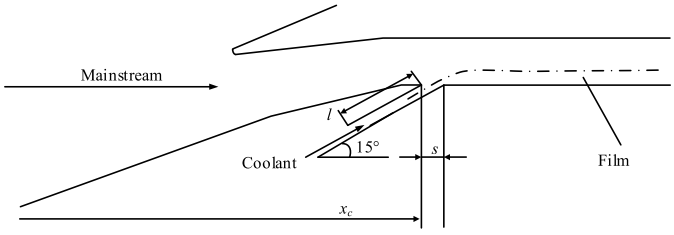

Fig. 2. Schematic of the scramjet isolator model with film cooling slot.

Table 1
Parameters of the freestream flow condition.

Ma_∞	T_∞ (K)	P_∞ (Pa)	TI
6.4	203.5	3968	0.01

utilized. Turbulence closure was achieved using the Shear–Stress Transport (SST) k–ω turbulence model that can capture the major features of the interaction between the shock wave and boundary layer, as well as the boundary layer separation. Uniform supersonic inflow was defined by specifying the boundary conditions at the inlet of the computational domain shown in Fig. 1(b). The details of the parameters of the freestream condition are listed in Table 1. The inlet Mach number was set to be $Ma_\infty = 6.4$. The boundary of the inflow was set to be a far pressure field. The variation of backpressure was achieved by adjusting the pressure outlet condition. The flow at the exit of the isolator is predominant supersonic outflow with no backpressure, the variables are completely extrapolated from their values at locations interior to the boundary. Otherwise, a prescribed pressure is used to simulate the influence of the throttle, and the remaining variables are extrapolated [38, 39]. For the cases with high backpressure, the subsonic flow region in the upstream boundary layer would grow rapidly. Therefore, the upstream flow condition can be affected by the prescribed pressure through the subsonic flow region in the boundary layer. In addition, a no-slip condition was enforced by setting the velocity components to zero on the solid walls; the walls were assumed to be adiabatic. These computations were conducted with the commercial computational fluid dynamics software FLUENT (Version 14.5).

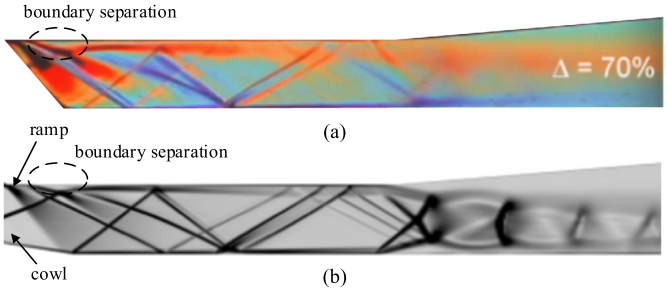

Fig. 3. Comparison of the Schlieren pictures in the isolator (a) experimental results obtained by Herrmann et al. [43]; (b) the corresponding simulation results obtained in the present study.

Similar numerical method was also adopted by Xu et al. [40] in the study of scramjet inlet under $Ma_\infty = 5.9$.

During the simulation, the air used in the main flow and coolant flow were considered to be a calorically perfect ideal gas. The specific heat capacity C_p was computed using the following piecewise-polynomial method [41]:

$$C_p = a_0 + a_1 T + a_2 T^2 + a_3 T^3 + a_4 T^4 + a_5 T^5 + a_6 T^6 + a_7 T^7 \quad (1)$$

where a_0–a_7 are polynomial coefficients with the corresponding value listing in Table 2.

In addition, the thermal conductivity λ of the air is determined by fitting the equations based on the NIST database [42]. The viscosity of air was solved according to the following Sutherland's formula [41]:

$$\mu = \mu_0 \left(\frac{T}{T_0}\right)^{3/2} \frac{T_0 + S}{T + S} \quad (2)$$

where μ_0 and T_0 are the reference viscosity and temperature, respectively. S is the Sutherland constant. The values of the parameters above are $\mu_0 = 1.716 \times 10^{-5}$, $T_0 = 273.11$ K, and $S = 110.56$ K.

2.3. Numerical validation

The experimental results obtained by Herrmann et al. [43] were used to validate the accuracy of the current numerical simulation. In their experimental studies, the inflow Mach number was set as $Ma_\infty = 2.0$ with angle of attack $\alpha = 10°$. The total temperature and total pressure were specified as 305 K and 540 kPa, respectively. A throttle was used in the experiments to simulate the backpressure of the isolator. The backpressure is 7 times as the static pressure of the inflow with 70% of the throttle closed. More details about the experimental setup can be obtained from Herrmann et al. [43]. Fig. 3 shows the comparison of Schlieren pictures with 70% of the throttle closed. It can be seen that the simulated flow fields in the isolator, including the shock wave pattern and boundary layer separation agree well with the experimental results. Therefore, our simulation can capture the primary flow structures in the scramjet isolator. In addition, the corresponding pressure distributions over the surface of the ramp and cowl are compared in Fig. 4. The good data agreement shown in Fig. 4 quantitatively reveals the accuracy of our simulation. A similar validation was also reported by Chang et al. [27] to investigate the effect of surface cooling on the performances of a hypersonic inlet.

Besides the flow characteristics in the isolator, the validation of the current numerical method for the film cooling was also performed in the present study. The compared film cooling experiments were conducted by Kanda et al. [6]. As shown in Fig. 5, the total temperature and the total pressure of the main flow with Mach number 2.35 were 280 K and 1400 kPa, respectively. The

Table 2
Polynomial coefficients in Equation (1).

T (K)	a_0	a_1	a_2	$a_3 \times 10^5$	$a_4 \times 10^8$	$a_5 \times 10^{12}$	$a_6 \times 10^{15}$	$a_7 \times 10^{19}$
100–1000	1161.482	−2.368819	0.01485511	−5.03490	9.928569	−111.1097	65.40196	−1.573588
1000–3000	−7069.814	33.70605	−0.0581276	5.421615	−2.936679	9.237533	−1.565553	1.112335

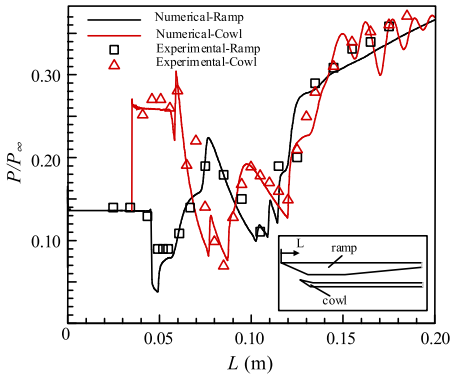

Fig. 4. Comparison of surface pressure distributions on ramp and cowl with 70% of the throttle closed.

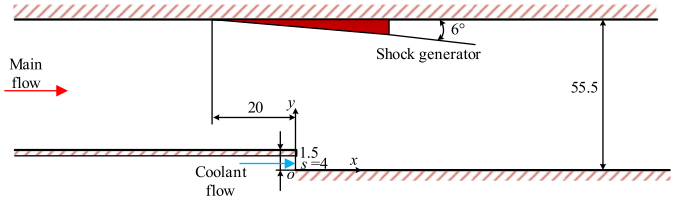

Fig. 5. Sketch of the film cooling experimental model (units: mm) [6].

coolant flow was injected into the main flow through a sonic nozzle. The total temperature and the total pressure of the coolant flow at the injector exit were 230 K and 220 kPa, respectively. Fig. 6 shows the comparison between the current simulation and the experimental study [6]. It can be found that the current simulation can reasonably predict the influences of shock wave on film cooling performances for both the aerodynamic characteristics (i.e., wall pressure) and the film cooling effectiveness.

In addition, three grid levels were employed to analyze the grid independency: coarse (50,972 cells), medium (142486 cells), and fine (447630 cells). To ensure the accuracy of the turbulent flow solution, the height of the first row of the cell for the three grid levels were set as 0.0174 mm, 0.01 mm, and 0.0058 mm, respectively. While the value of $y^+ < 5$ was realized for the coarse grid level, the values of $y^+ < 2$ and $y^+ < 1$ were achieved for the medium and fine grid level, respectively. Fig. 7 displays the comparison of pressure distributions over the model surfaces at three different grid levels. While the pressure distribution of the coarse grid level has considerable discrepancy in the region of $x \approx 470$–490 mm compared with the other two grid levels, the results of the medium grid level are quite similar to that of the fine grid level. In the studies of Peng et al. [9] and Xu et al. [40], the y^+ was controlled to be $y^+ < 3$. Therefore, all results shown herein are computed using the resolution of the medium grid level with $y^+ < 2$, which could reduce more than half of the computation times compared with that of the fine grid level. For the medium grid level, the minimum grid spacing was set at the exit of the cooling slot, which is approximately 0.01 mm in both x and y direction.

Table 3
Parameters of the coolant flow condition under different coolant Mach numbers.

P_c (Pa)	Ma_c	T_c (K)	m_c (kg/s)	m_c/m_{main} (%)	M
35000	2.4	300	0.16	3.2	0.69
35000	2.6	300	0.18	3.6	0.77
35000	2.8	300	0.20	4.0	0.86
35000	3.0	300	0.23	4.6	0.98
35000	3.2	300	0.25	5.0	1.07

Table 4
Parameters of the coolant flow condition under different coolant total temperatures.

P_c (Pa)	Ma_c	T_c (K)	m_c (kg/s)	m_c/m_{main} (%)	M
35000	3.0	300	0.23	4.6	0.98
35000	3.0	400	0.20	4.0	0.84
35000	3.0	500	0.18	3.6	0.75
35000	3.0	600	0.16	3.2	0.68

2.4. Coolant flow conditions

In the present study, the effects of injection Mach number (Ma_c) and coolant total temperature (T_c) on the film cooling effectiveness and aerodynamic performances of the scramjet isolator were investigated. The coolant flow was set to be fully turbulent at the entrance of injection slot with the turbulence intensity of 0.01. To avoid the unnecessary shock waves induced by the coolant flow, the static pressure of the coolant flow (P_c) was set to be the same as that of the main flow (P_{main}). Under this restriction, the mass flow rate (m_c) and resultant blowing ratio (M) can be determined when the injection Mach number and coolant total temperature are selected. The blowing ratio is defined as follows:

$$M = \frac{\rho_c U_c}{\rho_{main} U_{main}} \tag{3}$$

where ρ and U are the flow density and velocity, and the subscript c and $main$ indicate the coolant flow and the main flow.

During the simulation, the injection Mach number of the coolant flow changes from 2.4 to 3.2 with the blowing ratio varying from 0.69 to 1.07 correspondingly. The coolant total temperature changes from 300 K to 600 K with the blowing ratio varying from 0.98 to 0.68. In addition, the consumption of coolant air is a key parameter to evaluate the performance of a film cooling system. In the present study, the mass flow rate ratios between the coolant air and the air entering the inlet (i.e., m_c/m_{main}) are set to be less than 5% to control the consumption of coolant air. The details of the parameters of the studied coolant flow conditions are listed in Tables 3 and 4.

3. Results and discussion

3.1. Characteristics of film cooling efficiency on isolator surface

3.1.1. Effects of injection position on film cooling efficiency on isolator surface

As described above, four locations downstream the entrance of the isolator were selected as the film cooling injection position in the present study. Fig. 8(a) shows the comparison of the adiabatic wall temperature (T_{aw}) under different injection positions. The distribution of the adiabatic wall temperature without film cooling is

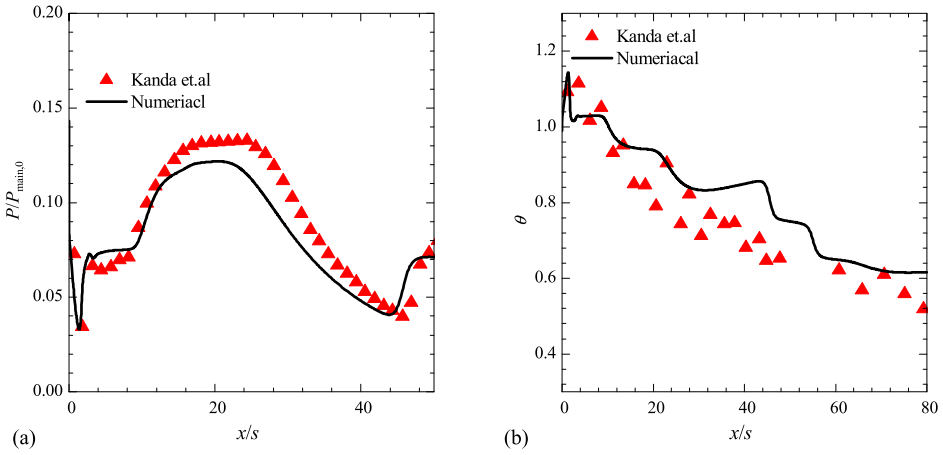

Fig. 6. Comparison of current simulation and experimental data in [6] (a) wall pressure; (b) film cooling effectiveness.

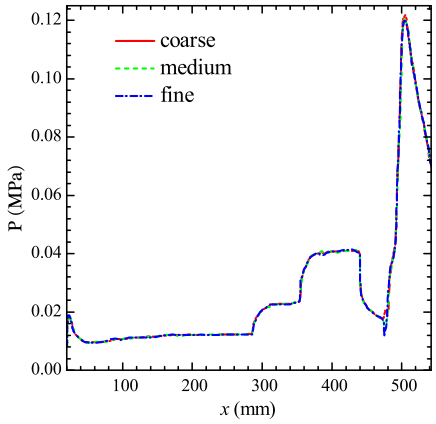

Fig. 7. Comparison of surface pressure distribution for different grid levels.

also plotted in the graph for comparison. It can be seen that the peak adiabatic wall temperature without film cooling on the isolator surface is approximately 1600 K, which is similar to that reported by Rodriguez [11]. The injection Mach number and coolant total temperature for the simulation cases shown in Fig. 8(a) were set to be 3.0 and 300 K with the corresponding blowing ratio of $M = 0.98$. In general, the introduction of film cooling could significantly decrease the wall temperature in a long distance downstream the injection slot. As shown in Fig. 10, the maximum wall temperature was reduced to 1100 K with film cooling. In addition, the adiabatic wall temperature increase continuously with the injection position moving downstream, thus indicating that the injection position exhibits a significant influence on the film cooling efficiency.

Besides the adiabatic wall temperature, the parameter of film cooling effectiveness (η) is typically used to evaluate the film cooling efficiency. According to the studies of Goldstein [44] and Juhany et al. [45], the film cooling effectiveness is given as follows:

$$\eta = \frac{T_{r,main} - T_{aw}}{T_{r,main} - T_{r,c}} \tag{4}$$

where T_{aw} is the local adiabatic wall temperature. $T_{r,c}$ and $T_{r,main}$ are the recovery temperatures of coolant flow and main flow, respectively. This definition of film cooling effectiveness is based on the adiabatic wall temperature and the recovery temperature. In the present study, $T_{r,main}$ is the adiabatic wall temperature measured along the surface without film cooling. $T_{r,c}$ is obtained by measuring the adiabatic wall temperature at the injection slot exit with the injected coolant flow.

The film cooling effectiveness under different injection positions are given in Fig. 8(b). With the continuous mixing of coolant flow with main flow, the air in main flow with a high temperature will finally reach the material surface at a downstream location. The region between this downstream location and the injection position is defined as the core cooling region (i.e., the surface is fully covered by the coolant gas with the cooling effectiveness close to 1.0). It can be seen that the length of the core cooling region decreases continuously with the injection moving downstream. Because the coolant gas has been used more efficiently in the core cooling region, the decrease in film cooling effectiveness behind the core cooling region becomes more significant for the upstream injection positions, as shown in Fig. 8(b).

It is known that the film cooling effectiveness is directly associated with the interaction between the coolant flow and the main flow. Fig. 9 shows the Mach number contour inside the isolator with the coolant flow injected from different positions. The Mach number contour without film cooling is also plotted for comparison. As shown in Fig. 9(e), it can be seen that the flow inside the isolator is actually a quite complex flow, including the flow phenomena of shock-shock interaction, shock-boundary layer interaction and boundary layer separation. As indicated by Zhang et al. [34] and Hombsch and Olivier [36], the injection coolant flow would block the main flow and induce additional shock waves and flow separation, which will deteriorate the main flow environments. Therefore, the film cooling for scramjet isolator should be introduced carefully to minimize the effect of injection flow on the main flow environments inside the isolator.

As shown in Fig. 2, the injection position of $x_c = 475$ mm is located at the entrance of the isolator. At this location, an angle exists between the inlet and isolator, thus leading to a downward deflection of the main flow when it enters the isolator. Obviously, this deflection of main flow could force the injected coolant flow to cover the isolator surface better, thus extending the length of the core cooling region, as shown in Fig. 8(b).

With the injection position moving to $x_c = 481$ mm and $x_c = 487$ mm, the beneficial effects of the deflection of main flow on film cooling efficiency for the case above (i.e., $x_c = 475$ mm) disappear, thereby resulting in the reduction in the core cooling region. More importantly, as compared in Figs. 8(b) and 9, it can be found that the film cooling effectiveness is closely related to boundary layer separation. When the boundary layer is separated, the corresponding film cooling effectiveness would decrease considerably. Therefore, with the injection position moving toward the boundary layer separation point, the length of the core cooling region would decrease accordingly. In addition, as shown in Figs. 9(b) and (c), a large flow separation appears in front of the injection posi-

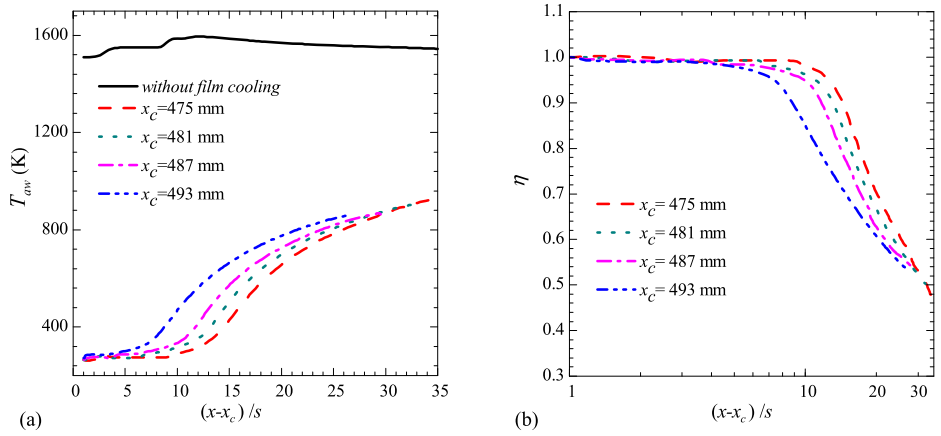

Fig. 8. Comparison of (a) adiabatic wall temperature and (b) film cooling effectiveness under different injection positions with the coolant flow condition of $P_c = 35000$ Pa, $Ma_c = 3.0$, and $T_c = 300$ K.

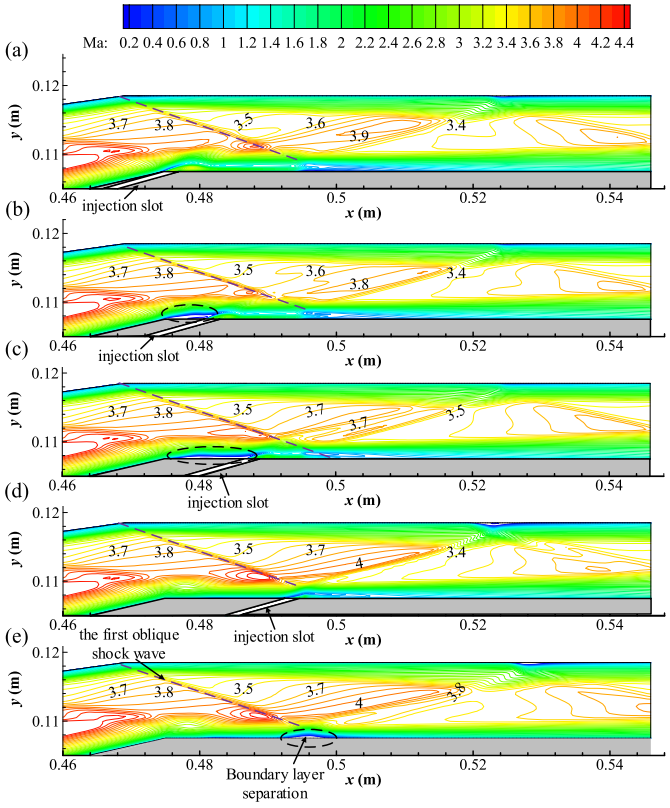

Fig. 9. Comparison of Mach number contour under different injection positions with the coolant flow conditions of $P_c = 35000$ Pa, $Ma_c = 3.0$, and $T_c = 300$ K (a) $x_c = 475$ mm; (b) $x_c = 481$ mm; (c) $x_c = 487$ mm; (d) $x_c = 493$ mm; (e) without film cooling.

tion, which is mainly caused by the blockage of the coolant flow. This flow separation will enhance the mixing of the downstream main flow with the coolant flow to further reduce the film cooling efficiency.

The injection position of $x_c = 493$ mm is located behind the first oblique shock wave. As shown in Fig. 9(d), the Mach number in main flow decreases significantly after this shock wave. The main flow with a lower Mach number cannot well restrict the coolant flow away from the surface. Therefore, the coolant flow after injection is much easier to separate from the surface and then mixing with the main flow, which leads to the significant decrease of the film cooling effectiveness. As shown in Fig. 8 (b), the film cooling effectiveness is much lower for the case of $x_c = 493$ mm compared to that of the other three injection positions. A similar finding was also reported in the study of Konopka et al. [46]. In addition, it can be found in Fig. 9(d) that the upstream flow separation caused by the blockage of the coolant flow shown in Figs. 9(b) and (c) disappears owing to the oblique shock wave located in front of the injection position. Further, the flow fields in front of the first oblique shock wave indicate no difference between the film-cooling case with $x_c = 493$ mm and the no-film-cooling case.

3.1.2. *Effects of injection Mach number on film cooling efficiency on isolator surface*

Fig. 10 shows the comparison between adiabatic wall temperature and film cooling effectiveness under different injection Mach numbers. The injection position of $x_c = 475$ mm was adopted based on the analysis above. The other detailed coolant flow conditions can be found in Table 3. It is noteworthy that while the static pressure of the coolant flow is set to be the same as the static pressure of the main flow, the blowing ratio is dominated by the injection Mach number and coolant total temperature. As listed in Table 3, under a constant coolant total temperature of $T_c = 300$ K, the blowing ratio of coolant flow would increase correspondingly with the increase in the injection Mach number.

As indicated by Goldstein et al. [44,47] and Taslim et al. [48], film cooling is the employment of a secondary fluid injected through discrete slots to thermally insulate a solid surface from mainstream gas flowing over it, which provides a cooling buffer between the hot mainstream gas and the solid surface. Therefore, the film cooling performance is mainly related to how firmly the coolant injected flow can remain attached to the surface to insulate the hot mainstream gas from the solid surface. The higher mass flow rate of the coolant flow would increase the film cooling efficiency if the coolant flow can remain attached to the surface. However, with the continuously increase in the blowing ratio, the coolant flow tends to take off from the surface owing to its high injection momentum compared to the main flow, resulting in a deteriorated cooling performance. Fig. 11 shows the Mach number contour inside the isolator with different injection Mach numbers. It can be seen that due to the effect of the main flow deflection at the entrance of the isolator, the injected coolant flow remains attached to the surface even under the highest injection Mach number simulated in this study (i.e., $Ma_c = 3.2$). In addition, a continuous decrease in the separation zone on the lower wall of the isolator is shown in Fig. 11 with the increase in injection Mach number, which would increase the film cooling effective-

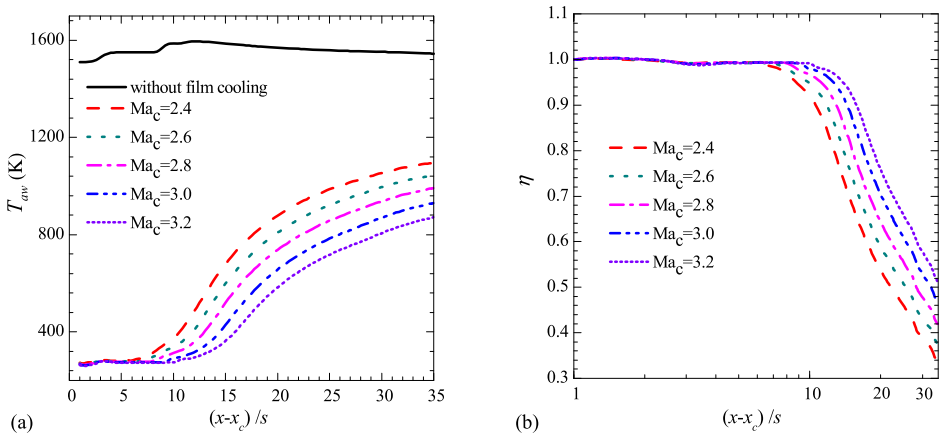

Fig. 10. Comparison of (a) adiabatic wall temperature and (b) film cooling effectiveness under different coolant Mach numbers with the coolant flow condition of $P_c =$ 35000 Pa, $T_c = 300$ K, and $x_c = 475$ mm.

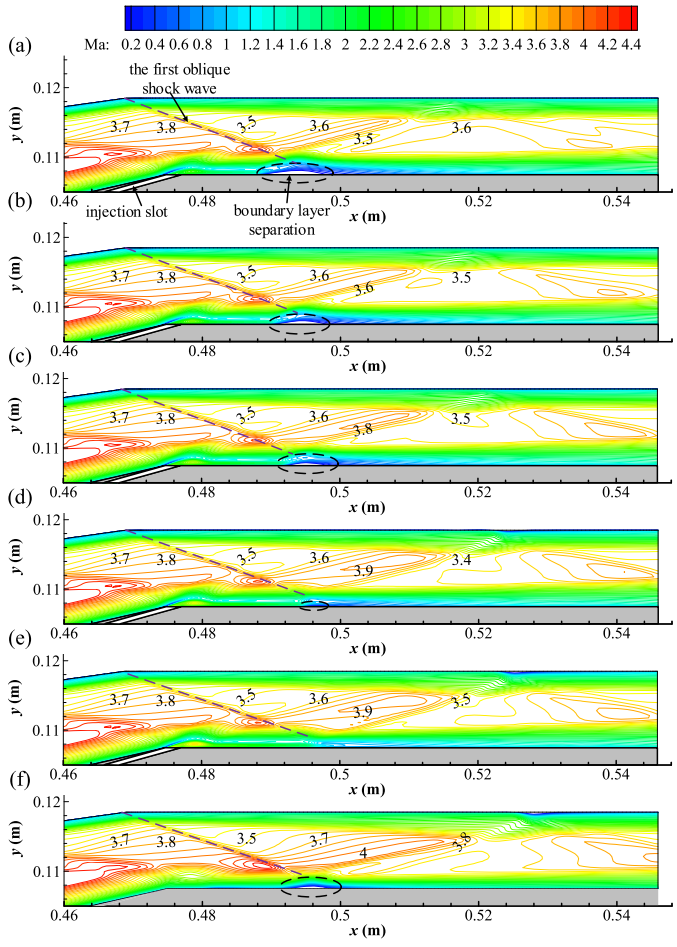

Fig. 11. Comparison of Mach number contour under different coolant Mach numbers with the coolant flow conditions of $P_c = 35000$ Pa, $T_c = 300$ K and $x_c = 475$ mm (a) $Ma_c = 2.4$; (b) $Ma_c = 2.6$; (c) $Ma_c = 2.8$; (d) $Ma_c = 3.0$; (e) $Ma_c = 3.2$; (f) without film cooling.

ness in the separation region significantly. Therefore, as expected, Fig. 10 shows that the core cooling region becomes longer with the increase in the injection Mach number and the corresponding blowing ratio. In addition, after the core cooling region, the deterioration in the film cooling efficiency with downstream distance is slower for a higher injection Mach number.

3.1.3. Effects of coolant total temperature on film cooling efficiency on isolator surface

Fig. 12 shows the comparison of adiabatic wall temperature and film cooling effectiveness under different coolant total temperatures. The injection position is selected at $x_c = 475$ mm. The detailed coolant flow conditions are listed in Table 4. Under a constant injection Mach number of $Ma_c = 3.0$, the blowing ratio of the coolant flow would decrease correspondingly with the increase in the coolant total temperature. As shown in Fig. 12(a), at the same location downstream of the injection slot, the adiabatic wall temperature shows an approximately linear increase with the coolant total temperature. The profiles plotted in Fig. 12(b) indicate that the film cooling effectiveness increase monotonously with a decrease in the coolant total temperature. The corresponding Mach number contours in the isolator are shown in Fig. 13. It can be seen that the separation zones under different coolant total temperatures are always smaller compared to the case without film cooling. In addition, a slight decrease in the separation zone can be found in Fig. 13 with the decrease in coolant total temperature, which would lead to the increase of the film cooling effectiveness.

3.2. Effect of film cooling on the aerodynamic performances of the isolator

3.2.1. Effects of injection position on the aerodynamic performances of the isolator

As shown in Fig. 9, the coolant flow injection exhibits a considerable influence on the boundary layer separation in the isolator. The boundary layer separation will cause the total pressure loss and deteriorate the performances of the isolator. More importantly, the severe boundary layer separation will lead to an engine unstart during the flight. Therefore, the separation region on the isolator surface is quantitatively recognized using the axial shear stress. As shown in Fig. 14(a), the region with axial shear stress below zero represents the boundary layer separation zone.

As shown in Figs. 9 and 14(a), a separation region can be found for the no-film-cooling case, which is caused by the interaction between the first oblique shock wave and boundary layer. It should be noted that $x_c = 475$ mm is located just at the entrance of the isolator, the downward deflection of main flow at this location could force the coolant flow to fully cover the isolator surface, which is similar to boundary layer blowing without injection angle. As indicated by Carroll and Dutton [12], boundary layer blowing can improve the velocity profile of the boundary layer, thereby weakening the boundary layer separation. This might be the rea-

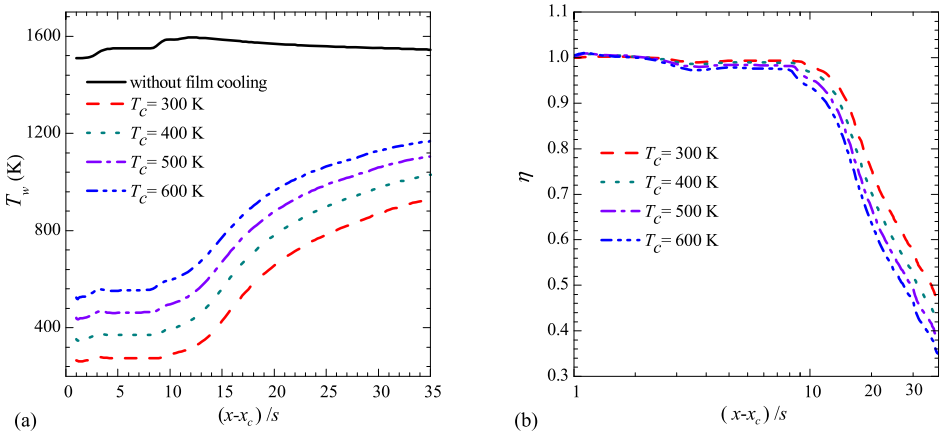

Fig. 12. Comparison of (a) adiabatic wall temperature and (b) film cooling effectiveness under different coolant total temperatures with coolant flow conditions of $P_c =$ 35000 Pa, $Ma_c = 3.0$, and $x_c = 475$ mm.

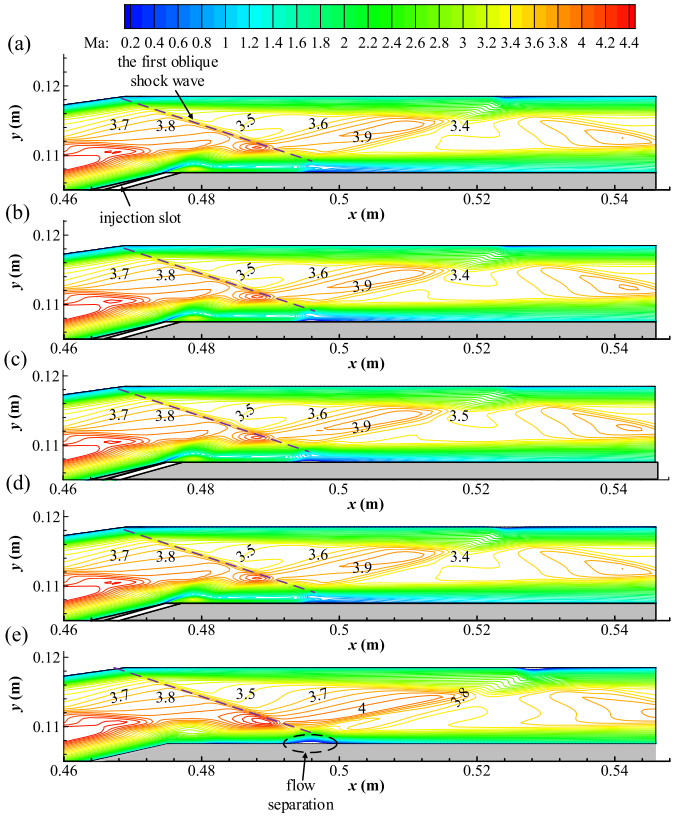

Fig. 13. Comparison of Mach number contour under different coolant total temperatures with the coolant flow conditions of $P_c = 35000$ Pa, $Ma_c = 3.0$, and $x_c = 475$ mm (a) $T_c = 300$ K; (b) $T_c = 400$ K; (c) $T_c = 500$ K; (d) $T_c = 600$ K; (e) without film cooling.

son for that the separation region shown in Fig. 9(a) is smaller compared to the no-film-cooling case shown in Fig. 9(e).

Except the injection position of $x_c = 475$ mm, the boundary layer separation phenomena are more obvious for other film cooling cases than that of the no-film-cooling case. For the cases of $x_c = 481$ mm and 487 mm, a large flow separation can be found between the injection position and isolator entrance due to the blockage effect of the coolant flow. In addition, the injection position of $x_c = 493$ mm is located behind the first oblique shock wave in the isolator. Owing to the upstream shock wave, the boundary layer separation could only occur in the region between the impinging point of the oblique shock wave and the injection position. As shown in Fig. 14(a), compared to the injection positions of $x_c = 481$ mm and 487 mm, the separation region caused by the blockage of the downstream coolant flow is much smaller with the injection position located at $x_c = 493$ mm.

It is known that the primary function of scramjet isolator is to prevent the scramjet inlet from disturbances that arise from the pressure increase in the scramjet combustor. A higher static pressure at the combustion entrance (i.e., static pressure at the exit of the isolator) pushes the shock wave train from moving forward to the entrance of the isolator. The engine unstart phenomenon will occur when the shock wave train is pushed out of the isolator. The maximum static pressure at the exit of the isolator that could guarantee the shock wave train inside the isolator is typically defined as the maximum backpressure. Obviously, the higher maximum backpressure allows for a more intense turbulent combustion, as well as a higher thrust of the scramjet engine. Increasing the maximum backpressure is effective in improving the aerodynamic performances of the scramjet engine. Fig. 14(b) shows the computed maximum backpressure under different injection positions. It can be seen in the introduction of film cooling can increase the maximum backpressure regardless of the injection position. Further, the behavior of the maximum backpressure is closely related to the flow quality inside the isolator. For the injection positions at $x_c = 481$ mm and 487 mm, the large flow separation between the injection position and the isolator entrance results in a reduced maximum backpressure compared with that of the injection position located at the isolator entrance (i.e., $x_c = 475$ mm).

In addition, as shown in Fig. 14(b), the highest maximum backpressure occurs with the injection position located at $x_c =$ 493 mm, which indicated that the boundary layer near the exit of the isolator can resist a higher static pressure at the combustion entrance for the injection position of $x_c = 493$ mm compared to the other upstream injection positions. In other words, while the film cooling efficiency is poor with the injection position located behind the oblique shock wave, the thrust performance of the scramjet engine can be improved significantly owing to the increased maximum backpressure.

3.2.2. Effects of injection Mach number on the aerodynamic performances of the isolator

The distributions of axial shear stress under different injection Mach numbers with a constant coolant total temperature ($T_c =$ 300 K) are given in Fig. 15(a). It is known that the injected coolant flow with a lower temperature will lead to lower speed of sound, thereby increasing the Mach number in the boundary layer. However, for the injection Mach number of $Ma_c = 2.4$, the boundary layer separation region behind the impinging of the oblique shock

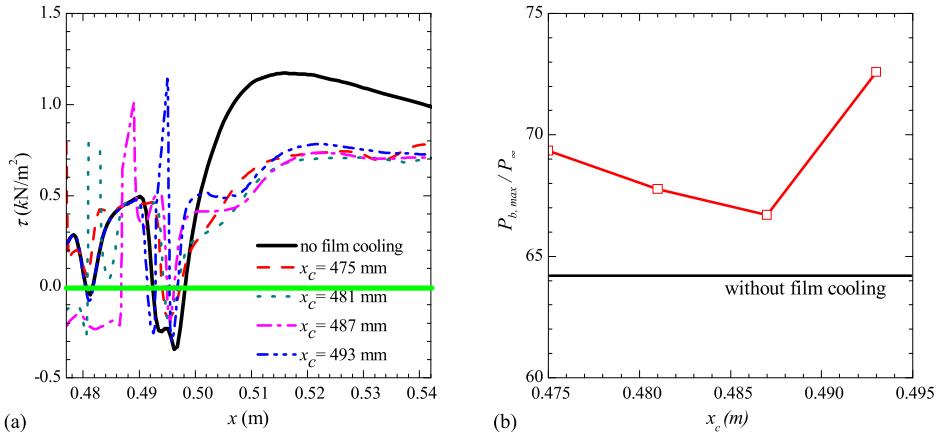

Fig. 14. Effects of injection position on the aerodynamic performances of the isolator with the coolant flow conditions of $P_c = 35000$ Pa, $Ma_c = 3.0$, and $T_c = 300$ K (a) distribution of axial shear stress; (b) maximum backpressure.

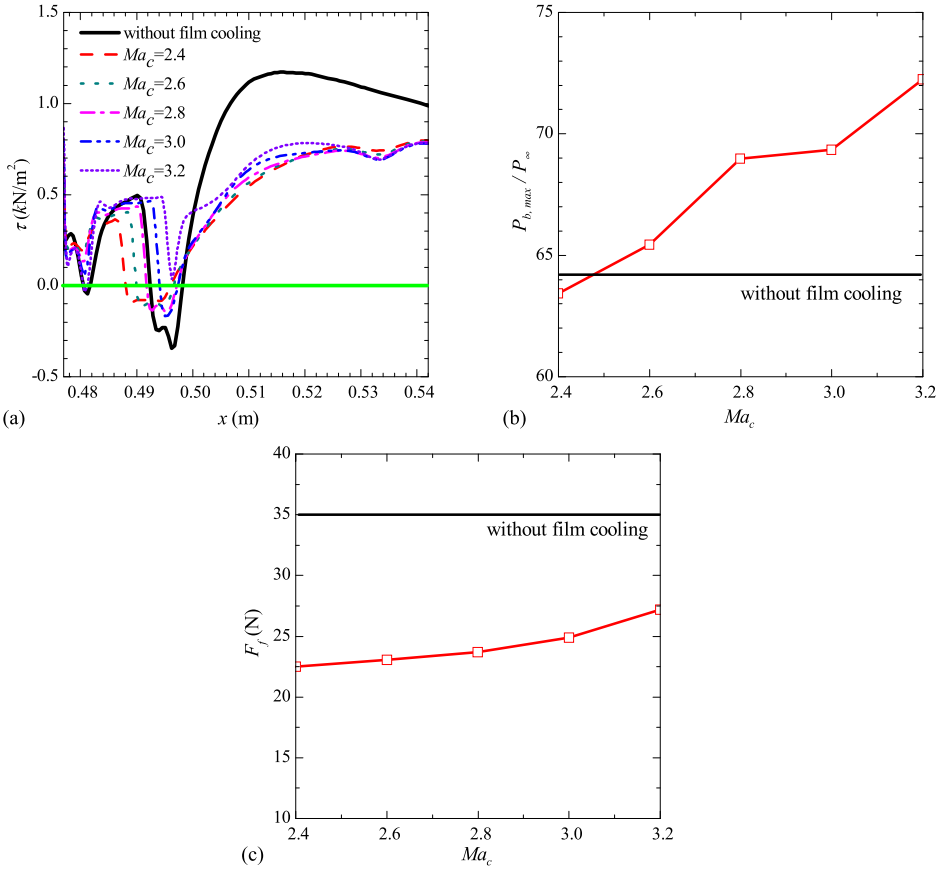

Fig. 15. Effects of coolant Mach number on the aerodynamic performances of the isolator with the coolant flow conditions of $P_c = 35000$ Pa, $T_c = 300$ K, and $x_c = 475$ mm (a) distribution of axial shear stress; (b) maximum backpressure; (c) friction drag.

wave is even larger than that of the no-film-cooling case. As shown in Table 3, the corresponding blowing ratio is only 0.69, indicating that the velocity of the injected coolant flow is much lower than that of the main flow. Therefore, the increase in boundary layer separation could be attributed to an extremely low injection Mach number (i.e., $Ma_c = 2.4$) that would decelerate the air speed in the boundary layer significantly. This decrease in air speed in the boundary layer is even greater than the increase in Mach number in the boundary layer caused by the decrease in temperature. Obviously, this decrease in air speed would reduce the ability of the boundary layer to resist the effect of downstream oblique shock wave. For the injection Mach number of $Ma_c = 2.6$, while the separation region (i.e., the region with the axial shear stress below zero) is close to that of the no-film-cooling case, the absolute value of the axial shear stress in the separation region is much lower compared to that of the no-film-cooling case. By further increasing the injection Mach number, as shown in Fig. 15(a), the boundary layer separation region decreases continuously. With the injection Mach number increasing to $Ma_c = 3.2$, the phenomenon of boundary layer separation disappears completely.

Because the boundary layer separation region is larger than that of the no-film-cooling case, the flow quality inside the isolator is deteriorated by the coolant flow with the injection Mach number of $Ma_c = 2.4$. As shown in Fig. 15(b), the corresponding

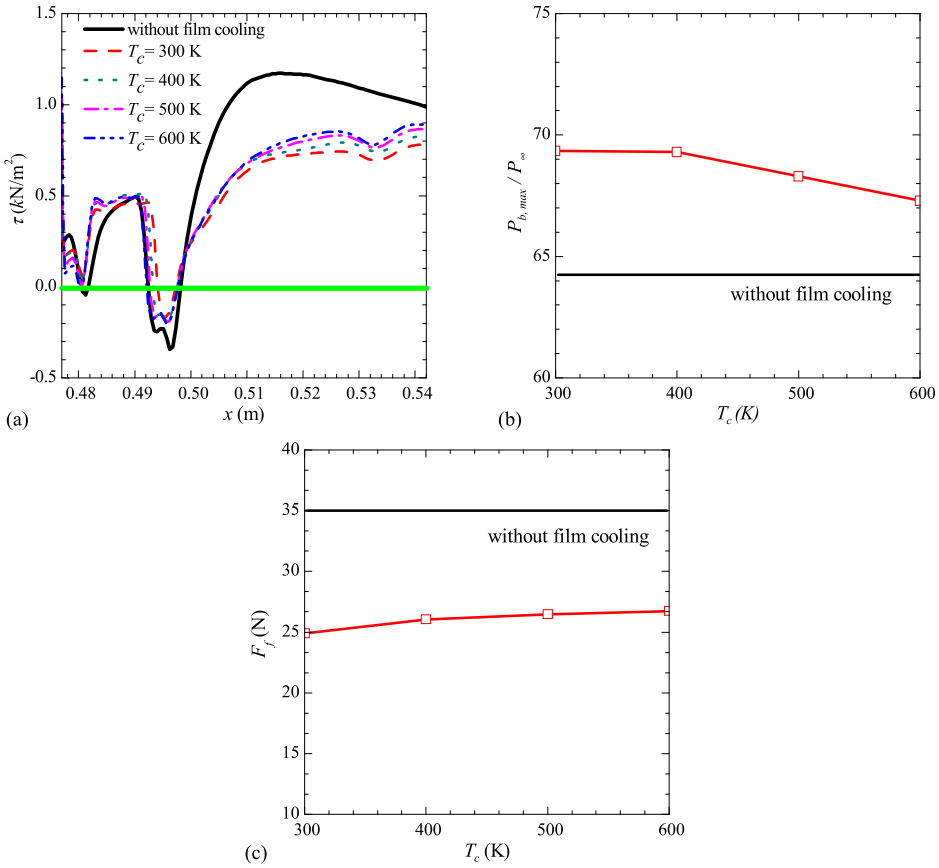

Fig. 16. Effects of coolant total temperature on the aerodynamic performances of the isolator with the coolant flow conditions of $P_c = 35000$ Pa, $Ma_c = 3.0$, and $x_c = 475$ mm (a) distribution of axial shear stress; (b) maximum backpressure; (c) friction drag.

maximum backpressure for the case of $Ma_c = 2.4$ is lower than that of the no-film-cooling case. The maximum backpressure was found to exceed that of the no-film-cooling case with the injection Mach number of $Ma_c = 2.6$ and increased continuously with the further increase in the injection Mach number. Therefore, it can be concluded that film cooling is not always beneficial for improving the maximum backpressure. There should be a critical value of the coolant Mach number for both the boundary layer separation and maximum backpressure. The coolant Mach number applied in film cooling should be high enough to ensure that the aerodynamic performances of the isolator cannot be deteriorated by the injected coolant flow.

As indicated by Chang et al. [27] and Rowan and Paull [49], owing to the decrease in flow temperature within the boundary layer, surface cooling causes the decrease in the corresponding flow viscosity within the boundary layer. Therefore, the friction drag on the isolator surface can be reduced by film cooling. The variation in friction drag on the lower surface of the isolator with injection Mach number is plotted in Fig. 15(c). As expected, the introduction of film cooling can decrease the friction drag on the isolator surface significantly, which could improve the thrust performances of the entire scramjet engine system. In addition, with more coolant flow injected into the boundary layer, the boundary layer will become fuller with a higher speed gradient near the wall. Therefore, as shown in Fig. 15(c), the friction drag exhibits a monotonous growth with the increase in injection Mach number.

3.2.3. Effects of coolant total temperature on the aerodynamic performances of the isolator

Fig. 16 (a) shows the distributions of axial shear stress under different coolant total temperatures with a constant coolant Mach number ($Ma_c = 3.0$). A continuously decreasing separation region with the separation point moving backward can be found clearly with the decreasing coolant total temperature. As mentioned above, the injection of coolant flow will increase the Mach number in the boundary layer. Obviously, the lower coolant total temperature will lead to a higher Mach number in the boundary layer that can better resist the effect of the downstream oblique shock wave.

As shown in Fig. 16(b), the maximum backpressure increases monotonously with the decrease in coolant total temperature, which is highly related to the change in the separation region on the isolator surface. The lower coolant total temperature can better improve the boundary layer separation in the isolator, thereby enhancing the isolator performance to better hold the shock wave train in the isolator. Compared with the no-film-cooling case, Fig. 16(b) shows that the increase in the maximum backpressure at the lowest coolant total temperature ($T_c = 300$ K) can reach approximately 8%. In addition, it is known that the flow viscosity is directly dependent on the flow temperature. The injected coolant flow with a lower temperature can better decrease the temperature in the boundary layer. Therefore, as expected, the friction drag on the lower surface of the isolator shown in Fig. 16(c) was found to decrease continuously with the decrease in coolant total temperature.

4. Conclusion

In the present study, a numerical investigation was conducted to evaluate the feasibility of applying the film cooling technique on the isolator of scramjet engine using a two-dimensional isolator model combined with a hypersonic inlet. The characteristics of the adiabatic wall temperature and film cooling effectiveness

under different coolant flow conditions (i.e., coolant Mach number, coolant total temperature, and injection position) were first analyzed. More importantly, the characteristics of maximum backpressure and friction drag of the isolator were analyzed to evaluate the effects of film cooling injection on the aerodynamic performances of the scramjet isolator. The detailed flow fields inside the isolator, especially the shock-boundary layer interaction and the separation of boundary layer on the lower surface of the isolator, were analyzed to gain further insight into the underlying physics to explore the feasibility and design paradigms for film cooling designs to protect the isolator surface.

The detailed flow field simulations indicated that the injected coolant flow primarily influenced the characteristics of the surface boundary layer, the downstream shock-boundary layer interaction, and the resultant boundary layer separation. It was found that the film cooling effectiveness was closely related to the boundary layer conditions. The film cooling efficiency decreased significantly when boundary layer separation occurred. With the injection position moving toward the boundary layer separation point, the corresponding film cooling efficiency was found to decrease considerably. In addition, owing to the blockage effect of the injected coolant flow, a large boundary layer separation was found between the injection position and isolator entrance. Therefore, the optimal aerodynamic performances of the isolator were obtained when the injection position was located at the entrance of the isolator.

A critical value of the coolant Mach number existed for both the boundary layer separation and maximum backpressure. The coolant Mach number applied in film cooling should be high enough to ensure that the aerodynamic performances of the isolator could not be deteriorated by the injected coolant flow. Above this critical value, the boundary layer separation region on the lower surface of the isolator was found to decrease gradually and finally completely disappeared. Meanwhile, the increase in the film cooling efficiency and maximum backpressure as well as the decrease in the friction drag were observed with the increase in the coolant Mach number.

A lower coolant total temperature resulted in a higher Mach number in the boundary layer, which could alleviate the downstream boundary layer separation. In addition, the coolant flow with a lower temperature could better cool the flow in the boundary layer, thereby reducing the flow viscosity. It was found that with the decrease in the coolant total temperature, the film cooling effectiveness and aerodynamic performances of the isolator were improved continuously by the coolant flow.

Declaration of competing interest

The authors declare that they have no competing interest.

Acknowledgement

Funding support from the National Natural Science Foundation of China (NSFC) through Grant 11872039 is gratefully acknowledged.

References

[1] D.M. Van Wie, S.M. D'Alessio, M.E. White, Hypersonic airbreathing propulsion, Johns Hopkins APL Tech. Dig. 26 (2005) 430–437.
[2] J. Qin, S. Zhang, W. Bao, Z. Jia, B. Yu, W. Zhou, Experimental study on the performance of recooling cycle of hydrocarbon fueled scramjet engine, Fuel 108 (2013) 334–340.
[3] X. Wu, J. Yang, H. Zhang, C. Shen, System design and analysis of hydrocarbon scramjet with regeneration cooling and expansion cycle, J. Therm. Sci. 24 (2015) 350–355.
[4] L. Taddeo, N. Gascoin, I. Fedioun, K. Chetehouna, L. Lamoot, G. Fau, Dimensioning of automated regenerative cooling: setting of high-end experiment, Aerosp. Sci. Technol. 43 (2015) 350–359.
[5] J.P. O'Connor, A. Haji-Sheikh, Numerical study of film cooling in supersonic flow, AIAA J. 30 (1992) 2426–2433.
[6] T. Kanda, F. Ono, M. Takahashi, T. Saito, Y. Wakamatsu, Experimental studies of supersonic film cooling with shock wave interaction, AIAA J. 34 (1996) 265–271.
[7] T. Kanda, F. Ono, Experimental studies of supersonic film cooling with shock wave interaction (II), J. Thermophys. Heat Transf. 11 (1997) 590–592.
[8] W. Peng, P.X. Jiang, Effect of shock waves on supersonic film cooling with a slotted wall, Appl. Therm. Eng. 62 (2014) 187–196.
[9] W. Peng, X.K. Sun, P.X. Jiang, Effect of coolant inlet conditions on supersonic film cooling, J. Spacecr. Rockets 52 (2015) 1456–1464.
[10] T. Kanda, G. Masuya, F. Ono, Y. Wakamatsu, Effect of film cooling/regenerative cooling on scramjet engine performances, J. Propuls. Power 10 (1994) 618–624.
[11] C.G. Rodriguez, Computational fluid dynamics analysis of the central institute of aviation motors/NASA scramjet, J. Propuls. Power 19 (2003) 547–555.
[12] B.F. Carroll, J.C. Dutton, Characteristics of multiple shock wave/turbulent boundary-layer interactions in rectangular ducts, J. Propuls. Power 6 (1990) 186–193.
[13] B.F. Carroll, J.C. Dutton, Computation of multiple normal shock wave/turbulent boundary-layer interactions, J. Propuls. Power 8 (1992) 441–448.
[14] C.J. Tam, K.C. Lin, D.L. Davis, R. Behdadnia, Numerical investigations on simple variable geometry for improving scramjet isolator performance, in: 42nd AIAA/ASME/SAE/ASEE Joint Propulsion Conference and Exhibit, 2006, AIAA-2006-4509.
[15] K.C. Lin, C.J. Tam, K. Jackson, P. Kennedy, R. Behdadnia, Experimental investigations on simple variable geometry for improving scramjet isolator performance, in: 43rd AIAA/ASME/SAE/ASEE Joint Propulsion Conference and Exhibit, 2007, AIAA-2007-5378.
[16] T. Kouchi, T. Mitani, G. Masuya, Numerical simulations in scramjet combustion with boundary-layer bleeding, J. Propuls. Power 21 (2005) 642–649.
[17] J. Chang, D. Yu, W. Bao, Y. Fan, Y. Shen, Effects of boundary-layers bleeding on unstart/restart characteristics of hypersonic inlets, Aeronaut. J. 113 (2009) 319–327.
[18] J. Chang, Y. Fan, Effects of boundary-layers bleeding on performance parameters of hypersonic inlets, Aircr. Eng. Aerosp. Technol. 81 (2009) 204–211.
[19] Y. He, H. Huang, D. Yu, Investigation of corner separation and suction control in constant area duct, Aerosp. Sci. Technol. 56 (2017) 70–82.
[20] R.F. Cuffel, L.H. Back, Flow and heat transfer measurement in a pseudo-shock region with surface cooling, AIAA J. 14 (1976) 1716–1722.
[21] K.C. Lin, C.J. Tam, D.R. Eklund, K.R. Jackson, T.A. Jackson, Effects of temperature and heat transfer on shock train structures inside constant-area isolators, in: 44th AIAA Aerospace Sciences Meeting and Exhibit, 2006, AIAA-2006-817.
[22] C. Fischer, T. Neuenhahn, H. Olivier, Numerical investigation of the isolator flow field of a scamjet engine with elevated wall temperatures, in: New Results in Numerical and Experimental Fluid Mechanics VII, Springer, 2010, pp. 415–422.
[23] C. Fischer, H. Olivier, Experimental investigation of wall and total temperature influence on a shock train, AIAA J. 52 (2014) 757–766.
[24] F.W. Spaid, J.C. Frishett, Incipient separation of a supersonic, turbulent boundary layer, including effects of heat transfer, AIAA J. 10 (1972) 915–922.
[25] L.H. Back, R.F. Cuffel, Shock wave/turbulent boundary-layer interactions with and without surface cooling, AIAA J. 14 (1976) 526–532.
[26] N.M.El-Hady.A.K. Verma, Instability of compressible boundary layers along curved walls with suction or cooling, AIAA J. 22 (1984) 206–213.
[27] J. Chang, W. Bao, D. Yu, Y. Fan, Y. Shen, Effects of wall cooling on performance parameters of hypersonic inlets, Acta Astronaut. 65 (2009) 467–476.
[28] V. Venkatesh, J. Sriraam, D.B. Vignesh, K. Subash, R.K. Velamati, A.R. Srikrishnan, B. Ramakrishnananda, S. Batchu, Studies on effusion cooling: impact of geometric parameters on cooling effectiveness and coolant consumption, Aerosp. Sci. Technol. 77 (2018) 58–66.
[29] C. Wang, J. Zhang, J. Zhou, Optimization of a fan-shaped hole to improve film cooling performance by RBF neural network and genetic algorithm, Aerosp. Sci. Technol. 58 (2016) 18–25.
[30] S.P. Choudhury, A. Suryan, J.C. Pisharady, A. Jayashree, K. Rashid, Parametric study of supersonic film cooling in dual bell nozzle for an experimental air–kerosene engine, Aerosp. Sci. Technol. 78 (2018) 364–376.
[31] P.R. Viswanath, L. Sankaran, R. Narasimha, A. Prabhu, P.M. Sagdeo, Injection slot location for boundary-layer control in shock-induced separation, J. Aircr. 20 (1983) 726–732.
[32] Y. He, H. Huang, D. Yu, Investigation of boundary-layer ejecting for resistance to back pressure in an isolator, Aerosp. Sci. Technol. 56 (2016) 1–13.
[33] A.M. Cary, J.N. Hefner, Film-cooling effectiveness and skin friction in hypersonic turbulent flow, AIAA J. 10 (1972) 1188–1193.
[34] S. Zhang, J. Qin, W. Bao, L. Zhang, Numerical analysis of supersonic film cooling in supersonic flow in hypersonic inlet with isolator, Adv. Mech. Eng. 6 (2015) 468790.
[35] S. Sivasegaram, J.H. Whitelaw, Film cooling slots: the importance of lip thickness and injection angle, J. Mech. Eng. Sci. 11 (1969) 22–27.
[36] M. Hombsch, H. Olivier, Film cooling in laminar and turbulent supersonic flows, J. Spacecr. Rockets 50 (2013) 742–753.

[37] K. Singh, B. Premachandran, M.R. Ravi, Experimental assessment of film cooling performance of short cylindrical holes on a flat surface, Heat Mass Transf. 52 (2016) 2849–2862.
[38] B.U. Reinartz, C.D. Herrmann, J. Ballmann, Aerodynamic performance analysis of a hypersonic inlet isolator using computation and experiment, J. Propuls. Power 19 (2003) 868–875.
[39] W. Huang, Z.G. Wang, M. Pourkashanian, L. Ma, D. Ingham, S. Luo, J. Lei, J. Liu, Numerical investigation on the shock wave transition in a three-dimensional scramjet isolator, Acta Astronaut. 68 (2011) 1669–1675.
[40] K. Xu, J. Chang, W. Zhou, D. Yu, Mechanism and prediction for occurrence of shock-train sharp forward movement, AIAA J. 54 (2016) 1403–1412.
[41] Fluent, 14.5 User's Guide, 2011, Chapter 7.
[42] E.W. Lemmon, A.P. Peskin, D.G. Friend, NIST 12: thermodynamic and transport properties of pure fluids, NIST standard reference database number 12, version 5.0. NIST, 2000.
[43] C.D. Herrmann, W.W. Koschel, K. Wolfgang, Experimental investigation of the internal compression inside a hypersonic intake, in: 38th AIAA/ASME/SAE/ASEE Joint Propulsion Conference and Exhibit, 2002, AIAA-2002-4130.
[44] R.J. Goldstein, Film cooling, Adv. Heat Transf. 7 (1971) 321–379.
[45] K.A. Juhany, M.L. Hunt, J.M. Sivo, Influence of injectant Mach number and temperature on supersonic film cooling, J. Thermophys. Heat Transf. 8 (1994) 59–67.
[46] M. Konopka, M. Meinke, W. Schroder, Large-eddy simulation of high Mach number film cooling with shock-wave interaction, Polyhedron 24 (16–17) (2013) 2315–2320.
[47] R.J. Goldstein, M.Y. Jabbari, Film cooling effectiveness with helium and refrigerant 12 injections into a supersonic flow, AIAA J. 8 (1970) 2273–2274.
[48] M.E. Taslim, S.D. Spring, B.P. Mehlman, Experimental investigation of film cooling effectiveness for slots of various exit geometries, J. Thermophys. Heat Transf. 6 (1992) 302–307.
[49] S. Rowan, A. Paull, Viscous drag reduction in a scramjet combustor with film cooling, in: 10th AIAA/NAL-NASDA-ISAS International Space Planes and Hypersonic Systems and Technologies Conference, 2001, AIAA-2001-1818.